Published in final edited form as:
*Bone*. 2009 September ; 45(3): 517–527. doi:10.1016/j.bone.2009.05.026.

# Apatite-coated Silk Fibroin Scaffolds to Healing Mandibular Border Defects in Canines

**Jun Zhao**[a], **Zhiyuan Zhang**[a], **Shaoyi Wang**[a], **Xiaojuan Sun**[c], **Xiuli Zhang**[b], **Jake Chen**[e], **David L. Kaplan**[d,*], and **Xinquan Jiang**[b,*]

[a] Department of Oral and Maxillofacial Surgery, College of Stomatology, Ninth People's Hospital, School of Medicine, Shanghai Jiao Tong University, Shanghai 200011, China

[b] Shanghai Research Institute of Stomatology, Shanghai Key Laboratory of Stomatology, Ninth People's Hospital, School of Medicine, Shanghai Jiao Tong University, Shanghai 200011, China

[c] Department of Oral and Maxillofacial Surgery, Affiliated Hospital of Ningxia Medical University, Ningxia 750004, China

[d] Department of Biomedical Engineering, Tufts University, Medford, MA 02155, USA

[e] Division of Oral Biology, Tufts University, Boston, MA 02111, USA

## Abstract

Tissue engineering has become a new approach for repairing bony defects. Highly porous osteoconductive scaffolds perform the important role for the success of bone regeneration. By biomimetic strategy, apatite-coated porous biomaterial based on silk fibroin scaffolds (SS) might provide an enhanced osteogenic environment for bone-related outcomes. To assess the effects of apatite-coated silk fibroin (mSS) biomaterials for bone healing as a tissue engineered bony scaffold, we explored a tissue engineered bony graft using mSS seeded with osteogenically induced autologous bone marrow stromal cells (bMSCs) to repair inferior mandibular border defects in a canine model. The results were compared with those treated with bMSCs/SS constructs, mSS alone, SS alone, autologous mandibular grafts and untreated blank defects. According to radiographic and histological examination, new bone formation was observed from 4 weeks post-operation, and the defect site was completely repaired after 12 months for the bMSCs/mSS group. In the bMSCs/SS group, new bone formation was observed with more residual silk scaffold remaining at the center of the defect compared with the bMSCs/mSS group. The engineered bone with bMSCs/mSS achieved satisfactory bone mineral densities (BMD) at 12 months post-operation close to those of normal mandible ($p>0.05$). The quantities of newly formed bone area for the bMSCs/mSS group was higher than the bMSCs/SS group ($p<0.01$), but no significant differences were found when compared with the autograft group ($p>0.05$). In contrast, bony defects remained in the center with undegraded silk fibroin scaffold and fibrous connective tissue, and new bone only formed at the periphery in the groups treated with mSS or SS alone. The results suggested apatite-coated silk fibroin scaffolds combined with bMSCs could be successfully used to repair mandibular critical size border defects

* Co-Corresponding author: Xinquan Jiang, Mailing address: 639 Zhizaoju Road, Ninth People's Hospital, School of Dental Medicine, Shanghai JiaoTong University, Shanghai 200011, China. Tel: +86-21-63135412, Fax: +86-21-63136856, xinquanj@yahoo.com.cn; David L. Kaplan, Mailing address: 4 Colby Street, Department of Biomedical Engineering, Tufts University, Medford, MA 02155, USA. Tel: +1 617 627 3251, Fax: +1 617 627 3231, david.kaplan@tufts.edu(D.L. Kaplan).

and the premineralization of these porous silk fibroin protein scaffolds provided an increased osteoconductive environment for bMSCs to regenerate sufficient new bone tissue.

### Keywords

Tissue engineering; Silk; Apatite; Bone marrow stromal cells; Canine

## Introduction

Mandibular bony defects, resulting from tumors, trauma, congenital malformations or reconstructive surgery are challenging problems for oral and maxillofacial surgeons. Autogenous bone grafts, particularly vascularized bone grafts, are currently the preferred method of repair because of the increased osteogenic potential and resistance against infection [1,2]. However, the main disadvantages associated with the use of autografts include finite amounts of autogenous bone as well as donor site morbidity. Similarly, the use of allografts are associated with potential for disease transmission, immunogenic response, and nonunion [3,4]. Fortunately, tissue engineering has emerged as a novel approach in this field to enhance bone regeneration instead of autografts and allografts. In this approach, highly porous scaffolds serve as the osteoconductive growth substrate for osteoblasts or osteoprogenitor cells and allow nutrients to permeate to support cell growth and differentiation leading to new bone tissue formation in three dimensions [5].

The most useful tissue engineering scaffold materials should be biocompatible, porous, and provide appropriate mechanical properties [6-9]. Degradable polymeric scaffolds used for bone tissue engineering, such as poly(lactic-co-glycolic acid) or poly-lactic acid, can induce inflammation due to the acidity of their hydrolysis products [10,11]. Meanwhile, matching mechanical properties of native bone remains a challenge for most polyesters [12,13]. At the same time, calcium phosphate bioceramics, such as hydroxyapatite (HA) and tricalcium phosphate (TCP) have been widely used for bone regeneration applications. However, the inherent brittleness of calcium phosphates impedes their use as the exclusive graft material in weight-bearing or large defects [14,15]. Therefore, there is a need to identify alternate biomaterials to overcome these limitations and meet the challenging combination of appropriate chemistry, mechanical features, morphology and structure to promote cell adhesion, differentiation, and synthesis of new bone matrix for bone regeneration.

To this end, there is growing interest in the development of ceramic-biodegradable polymer composites for use in bone repair [16-20]. Bioactive ceramics are known to enhance osteoblast differentiation as well as osteoblast growth [21,22]. These systems have been used in dental and orthopedic surgery to fill bone defects and to coat metallic implant surfaces to improve implant integration with the host bone. Biological apatite comprises a range of minerals found naturally in bone and has osteoconductive and osteophilic properties [23-27].

Silk fibroin has been used for decades as suture material, and recent studies have demonstrated the utility of silk matrices in film, nanofiber, and porous matrix formats for tissue engineering with stem cells, and for the formation of cartilage [28] and bone [29-31]. These scaffolds present established biocompatibility, impressive mechanical features and slow degradability [32], but do not provide osteoconductive properties. Apatite-coated silk scaffolds, however, can combine the osteoconductive properties of bioceramics with the mechanical resilience of polymers. Silk scaffolds combined with apatite promoted cellular attachment and bone nodule formation *in vitro*, providing an appropriate osteogenic environment for tissue engineering [33].

The goal of the present study was to determine the osteogenic features of the apatite-silk composite materials as a tissue engineered bony scaffold *in vivo.* To address this goal, bMSCs were seeded into the scaffolds to repair bilateral inferior mandibular border defects measuring 2 cm × 1 cm in a canine model. The effects of the bMSCs seeded apatite-silk composites were compared with additional study groups including silk scaffolds (without apatite) seeded with bMSCs, apatite modified silk scaffolds without the bMSCs, plain silk scaffolds without apatite modification or the addition of bMSCs, and untreated defects. To our knowledge, this is the first report to utilize these modified silk scaffold composite systems for the repair of mandibular bony defects in a large animal canine model.

## Materials and methods

### Animals

A total of 14 adult male mongrel dogs in healthy condition, aged 18 months old, each weighing from 15.0-20.0 kg were used in this study. All animals were obtained from the Ninth People's Hospital Animal Center (Shanghai, China) and treated under the same standard laboratory conditions, and were given the same soft diet. All the experimental protocols involving the use of dogs were approved by the Animal Care and Experiment Committee of Ninth People's Hospital affiliated to Shanghai Jiao Tong University, School of Medicine.

### bMSCs isolation, culture and osteoblastic characteristics

Under general anesthesia with ketamine (10 mg/kg) and xylazine (4 mg/kg), around 4 ml of autologous bone marrow were harvested by needle aspiration from the iliac crests of each dog and transferred into a pre-heparinized centrifuge tube. The specimens were cultured in Dulbecco's Modified Eagle Medium (DMEM) (Gibco BRL, Grand Island, NY, USA) supplemented with 10% fetal bovine serum (FBS, Hyclone, Logan, UT, USA), containing 100 units/ml of penicillin, 100 units/ml of streptomycin and 2 mM L-glutamine (Sigma, St. Louis, MO, USA). After 5 days, non-adherent cells were removed and fresh medium was added. The remaining adherent cells were mainly mesenchymal stromal cells. The culture medium was then changed every 2-3 days. Hematopoietic cells, which did not adhere to dishes, were discarded. When bMSCs reached 80-90% confluence, cells were detached with trypsin/EDTA (0.25% w/v trypsin, 0.02% EDTA) and then subcultured in 100 mm dishes. After the first passage, the following 3 supplements for inducing osteogenesis were added: $10^{-8}$ M dexamethasone, 50 μg/ml L-2-ascorbic acid and 10 mM β-glycerophosphate (Sigma, St. Louis, MO, USA). The cells were then incubated continuously at 37 °C in a humidified atmosphere of 95% air and 5% $CO_2$. Cells at passage 2-3 were used for all experiments.

After culturing in the induced medium for 14 days, the cells were measured by alkaline phosphatase (ALP) staining and von Kossa. Briefly, cells were fixed for 10 minutes at 4 °C and incubated with a mixture of naphthol AS-MX phosphate and fast blue BB salt (ALP kit, Hongqiao, Shanghai, China) [34]. The Von Kossa staining was performed by fixing the cells in 70% ethanol and staining with 5% silver nitrate, and 5% $Na_2SO_3$ [35].

### Preparation of silk fibroin aqueous solution

The aqueous silk fibroin solution was prepared by our previously published procedures [36]. Cocoons of *Bombyx mori* were boiled for 20 min in an aqueous solution of 0.02 M $Na_2CO_3$, and then rinsed thoroughly with distilled water to extract the glue-like sericin proteins. The extracted silk fibroin was dissolved in 9.3 M LiBr solution at 60 °C for 4 h, yielding a 20 w/v % solution. This solution was dialyzed in distilled water using a Slide-a-Lyzer dialysis cassette (MWCO 3,500, Pierce) for 2 days. The final concentration of silk fibroin aqueous solution was ca. 8 w/v%, which was determined by weighing the remaining solid after drying. All solutions were stored in a refrigerator at 7-8 °C before use to avoid premature precipitation.

### Preparation of silk fibroin-polyaspartic acid porous scaffolds

For the preparation of the polymer solutions the required amount of polyaspartic acid solution (20 wt%) in water was added to silk fibroin aqueous solution (8.0 wt%) with mild stirring for 2 min. The blend ratio of silk fibroin/polyaspartic acid was 80/20 (w/w), based on our prior studies [37]. Aqueous-derived silk fibroin scaffolds were prepared using our previously published methods [38], by adding 4 g of granular NaCl (particle size; 850-1000 μm) into 2 ml of silk fibroin-polyaspartic acid solution in disk-shaped containers which were then covered and left at room temperature. After 24 h, the containers were immersed in water and the NaCl extracted for 2 days.

### Mineralized scaffolds

The alternate soaking process was used to grow apatite on the silk fibers [37]. First, silk fibroin-polyaspartic acid scaffolds (20 mm in length, 10 mm in height and 6 mm in thickness) with pore size of 500-600 μm were soaked in 20 ml of 200 mM $CaCl_2$ solution (buffered with 50 mM Tris·HCl, pH 7.4) for 20 min at 37 °C and washed twice with 200 ml of distilled water. The silk fibroin-polyaspartic acid scaffolds were then transferred to 20 ml of 120 mM $Na_2HPO_4$ solution, soaked for 20 min at 37 °C and washed twice with 200 ml of distilled water. After soaking cycles were repeated 7 times, and the mineralized scaffolds were freeze-dried [39].

### Construction of cell material complex used in vitro and in vivo

For cell seeding, osteogenically induced bMSCs were detached from culture dishes, centrifuged to remove supernatant, and then resuspended in the culture media without serum at a density of $5\times10^7$ cells/mL. Cells in suspension were slowly injected into the silk scaffolds using a syringe (400 μl/scaffold) to generate a cell-material complex for the mandible surgeries *in vivo*. In a parallel experiment, 3 × 3 × 3 mm cuboids were prepared and seeded with bMSCs at an identical cell density *in vitro*. After 14 days of incubation, these *in vitro* grown constructs were fixed in 2% glutaric dialdehyde and then characterized by scanning electron microscopy (SEM) (PHILIPS XL 30 ESEM, Philips, Eindhoven, The Netherlands).

### Surgical procedure

The animals were anesthetized through intramuscular injection of ketamine (10 mg/kg) and xylazine (4 mg/kg) and then placed in a supine position. The inferior mandibular border was exposed through a submandibular skin incision. The mandibular periosteum was carefully dissected. With a bur that was cooled continuously by 0.9% saline solution irrigation, bilateral inferior mandibular border full-thickness defects of 20 mm × 10 mm under the premolars were made between the mental foramen and the mesial root of the first molar surgically in each animal (Fig. 1). The inferior alveolar neurovascular bundle was cut off and stanched by filling bone wax into mandibular canal. Then, a titanium plate was secured in place with four screws (two at the mesial side and two at the distal side). Twenty inferior mandibular border defects from 10 mongrel dogs were generated and randomly allocated into the following graft study groups: (1) SS alone (n = 4); (2) mSS alone (n = 4); (3) SS with bMSCs (n = 4); (4) mSS with bMSCs (n = 4) and (5) resected autogenous bone (n = 4) (Fig. 2). To ensure that the bony defects were critically sized, four defects in another two animals were left untreated as blank controls (n=4).

### Radiographic and dual energy X-ray absorptiometry analyses

Mandibular radiograms were obtained under general anesthesia at 1, 3, 6 and 12 months post-operation. Maxillofacial CT images were obtained and the three-dimensional images were reconstructed using a multi-slice spiral CT (GE Lightspeed Ultra 16, Milwaukee, WI, USA) at 12 months post-operation. For dual energy X-ray absorptiometry (DXA) analysis, animals

were sacrificed at 12 months post-operation. The mandibles were harvested and the titanium plates were removed. The local bone mineral densities (BMD) were measured on a DXA system (Hologic Discovery A, Bedford, MA, USA). To determine the radiopacity and BMD value of normal mandible and compare them with different constructs, four normal mandible samples from two extra animals with the same condition were enrolled.

### Histological and histomorphological analysis of bone regeneration

After the BMD tests, all the samples were processed for histological examination. The repaired mandible was bisected into the buccal and lingual halves along the maximal sagittal plane, then fixed in buffered 10% formalin for 72 h. Lingual half was decalcified in 15% formic acid for 8–12 weeks and then embedded in paraffin. Tissue sections 5 μm thick were then obtained for hematoxylin and eosin (H&E) staining and analyzed histomorphometrically using a PC-based image analysis system (image-Pro Plus™, Media Cybernetic, Silver Springs, MD, USA). The percentages of new bone area and residual scaffold among the initially repaired area were calculated by the average value of the three parallel slices selected from three equally divided paraffin samples defined at buccolingual directions. The mean value of the three measurements was calculated for each graft and they were further used to calculate mean values for each group. A Buccal half was used for undecalified fluorescent labeling tests for calcium (data not shown).

### Statistical analysis

Statistically significant differences ($p<0.05$) between the groups were measured by ANOVA and SNK post hoc or Kruskal-Wallis non-parametric procedure followed by Mann-Whitney U test for multiple comparisons based on the normal distribution and equal variance assumption test. All statistical analysis was carried out using a SPSS statistical software package (version 12; SPSS, Chicago, Ill, USA). All the data are presented as mean ± standard deviation.

## Results

### Cell culture, ALP and von Kossa staining

Cell clones formed 5-7 days *in vitro* after initial seeding, and reached confluence after approximately 10-12 days. After subculture, bMSCs showed a typical fibroblastic phenotype and were used for further studies (Fig. 3A). Two weeks after culture in osteogenic medium, areas of ALP-positive staining (Fig. 3B) and calcium deposits (Fig. 3C) were observed, which suggested that the bMSCs differentiated into osteoblastic cells.

### Growth of osteogenically induced bMSCs on scaffolds

The microstructure of scaffolds and the interactions of the bMSCs within the 3D scaffolds were evaluated by SEM. A thin uniform layer of apatite coating was visible on the surface of mineralized silk scaffold (Fig. 4A) compared with the plain silk scaffold (Fig. 4B). After 14 days culture in osteogenic media with bMSCs, the seeded cells attached to the plate-like apatite-coated silk scaffold surfaces, suspended between the backbones of scaffolds and grew along the pores of the scaffolds. The cells grew tightly to each other and reached confluence with abundant fibril networks of extracellular matrix and mineralized nodules deposited on the scaffolds (Fig. 4C). Visually, less extracellular matrix and mineralized nodules formed on the plain silk scaffolds (Fig. 4D) than on the hybrid apatite-coated silk scaffolds. Additionally, the results suggested that these composite biomaterials were suitable for the proposed *in vivo* studies as they facilitated bMSCs attachment, spreading and growth.

### General observations

All animals survived the surgical procedure. Slight post-surgical edema was observed at the recipient site in each animal and this disappeared 4 to 6 days after the procedure. There was no sign of infection at any time.

### Radiographic and dual energy X-ray absorptiometry analyses

To follow new bone formation and the development of bone unions within the defects, X-ray images were taken at 1, 3, 6 and 12 months post-operation. Representative photographs of each group are shown in Fig. 5. In the experimental group with bMSCs/mSS constructs, little calluses were observed in the defect 1 month post-operation (Fig. 5A), and more calluses were observed at 3 months (Fig. 5B). At 6 months post-operation, the volume and radiopacity of newly formed bone were highly increased (Fig. 5C); at 12 months, the radiopaque shadow had completely expanded to fill the mandibular defect (Fig. 5D) and the radiopacity was close to that of proximal normal mandible (Fig. 5J). By contrast, in the group with implanted bMSCs/SS constructs the radiopacity also increased but the new bone formation failed to cover the defects completely even at 12 months after implantation (Fig. 5E). Only little calluses were observed near the defect margin in the mSS (Fig. 5F) and SS alone (Fig. 5G) groups at 12 months. Calcified tissues mainly grew in from the host bones. As a positive control, the autograft group showed some callus formation at the junction sites at 1 month post-operation (data not shown). The bone density continuously increased with newly formed bone after 12 months (Fig. 5H). In the blank control, the untreated defects did not repair even at 12 months (Fig. 5I). The statistical analysis of the healed areas among the different groups is shown in Fig. 6A. The bMSCs/mSS group showed a healing percentage of 89.1±9.1%, which was higher than the bMSCs/SS group 76.3±11.2% ($p<0.05$). Whereas the mSS and SS alone groups showed 40.3±3.9% and 36.0±4.8%, respectively.

To quantify the calcification of repaired mandibles, local bone mineral densities (BMD) of all animals were measured on DXA at 12 months post-operation (Fig. 6B). The bMSCs/mSS group showed relatively high BMD of 0.45±0.06 g/cm$^2$, which was similar to the normal mandibles (0.49±0.02 g/cm$^2$, $p>0.05$). In bMSCs/SS group, the local BMD was 0.39±0.03 g/cm$^2$, which was not significantly different from bMSCs/mSS group ($p>0.05$). But the local BMD of this group was lower than normal mandibles ($p<0.05$). Whereas in mSS and SS alone groups, the local BMDs were 0.22±0.04 and 0.21±0.03 g/cm$^2$, respectively, which were significantly lower than that of the bMSCs/mSS and bMSCs/SS grafts ($p<0.01$). Meanwhile, the BMD of the autograft group was higher than other four groups (0.52±0.04 g/cm$^2$, $p<0.05$). The mineralized silk scaffold or the plain silk scaffold blocks alone with the same size as those implanted did not display any detectable BMD value in DXA tests, so the contribution to the total density was negligible.

### 3D reconstruction and gross view

To detect the three-dimensional structure of repaired mandiblar border defects, 3D-CT images of the lingual side were taken at 12 months post-operation. Representative images from each group are presented in Fig. 7. In the experimental group with bMSCs/mSS constructs, the mandible defects were completely repaired and the border of the new bone was close to the normal inferior mandibular border. The mandible contour was reconstructed (Fig. 7A). In the group with bMSCs/SS constructs, the mandible defects were partially repaired and the new bone formation was a little less than the bMSCs/mSS group. The inferior part of the defects failed to repair completely (Fig. 7B). However, in the group treated with mSS (Fig. 7C) or SS alone (Fig. 7D), only minimal calluses were observed at the margins of the defects. In the autograft group, the defects were completely repaired (Fig. 7E). While, in the blank control, no obvious bone formation was observed even at 12 months (Fig. 7F).

In correlation with radiographic and 3D-CT analyses, gross view at buccal side of the mandible repaired with either bMSCs/mSS constructs (Fig. 8A) or autologous bone (Fig. 8E) showed bony healing at 12 months post-operation. The borders of repair mandibles were very close to that of normal mandibles. In the bMSCs/SS group, part of the mandible defects were healed but the inferior of the defects remained unfilled completely (Fig. 8B). On the contrary, in the mSS (Fig. 8C) or SS alone (Fig. 8D) groups, bony callus were poorly formed at the defect margins.

### Histological examination and histomorphological analysis

To further confirm the above findings, histology of decalcified tissue sections with H&E staining at 12 months post-operation was conducted. In the bMSCs/mSS group, the defect site had been completely filled with new bone (Fig. 9A1). Substantial new bone formation was observed without a clear boundary between newly formed tissue engineered bone and native bone (Fig. 9A2). The silk fibroin scaffolds lost their structural integrity during this time frame, with separate small pieces left that were almost filled by irregular osteon formation in the repaired area. Blood vessels were formed accompanied with the bony ingrowth (Fig. 9A3). In the bMSCs/SS group, new bone formation was observed with more residual silk scaffold at the center of the defect (Fig. 9B1) compared with the bMSCs/mSS group. Silk fibroin scaffolds still held their pore structure and were unfilled by enough newly formed bone (Fig. 9B3). Although the newly formed bone at the defect area were remodeled and were histologically similar to the bMSCs/mSS group, the area of new bone formation was less than with the bMSCs/mSS group. In mSS (Fig. 9C1-C3) and SS alone (Fig. 9D1-D3) groups, bony defects were still present in the center, and new bone only formed at the periphery. The scaffolds in the center of these two groups failed to completely degrade and coexisted with fibrillar matrices. Despite some bone ingrowth from the interface region, no sufficient bone formation was seen in the central area. In the autograft group (Fig. 9E1-E3), a bony-union was observed with mature lamellar bone coexisting in the repaired area. The percentage of the newly formed bone among the initially repaired area (shown with the blue broken line) was calculated by histomorphometrical analysis (Fig. 10A). At 12 months post-operation, the percentage of newly formed bone for bMSCs/mSS group was 80.20±5.85%, which was much higher than that in the bMSCs/SS group 68.34±5.70% ($p<0.01$). No significant difference was found with the bMSC/mSS group compared with the autograft group 84.45±2.75% ($p>0.05$). While the percentages of newly formed bone for SS and mSS alone groups were 31.71±4.89% and 30.78 ±2.89%, respectively. The percentage of residual scaffold among the initially repaired area (Fig. 10B) was 9.28%±1.74% in the bMSCs/mSS group, 15.73%±3.79% in the bMSCs/SS group, 4.03±1.34% in the SS group and 5.18%±1.02% in the mSS alone group, respectively. There was significant difference between each group except for the difference between SS and mSS alone groups.

## Discussion

The goal of the present study was to evaluate a new premineralized degradable protein composite system with enhanced repairing effects as a tissue engineered scaffold for inferior mandibular border defects. The aqueous-derived porous silk fibroin scaffolds, which were premineralized with apatite, combined with bMSCs were implanted into the critical sized margin defects of the canine mandible, and osteogenesis was compared to defects treated with bMSCs/SS constructs, mSS alone, SS alone, autologous mandibular grafts and untreated control defects.

Silk fibroin is the structural, hydrophobic, high molecular weight protein isolated from the cocoon of *B. mori* [40,41] that has emerged as a novel scaffold for tissue engineering. This biomaterial is biocompatible [32,36,42,43], offers distinguishing mechanical properties and

slow degradability when compared to other naturally derived or degradable polymeric biomaterials [44]. Critical sized cranial and femur defects in murine models have been healed using silk scaffolds (SS) with human mesenchymal stem cells (hMSCs) that had previously been differentiated along an osteoblastic lineage for up to 5 weeks *in vitro* [45,46]. Natural bone, which contains inorganic as well as organic phases, are formed by a series of complex events involving mineralization with calcium phosphate in the form of hydroxyapatite (HAP) on extracellular matrix proteins. Besides, being a natural component of human bone, apatites have been shown to mediate and promote bone regeneration around wounds [47]. Biomaterial scaffolds with apatite coatings have been shown to promote bone in-growth in defects in dog and goat femurs, enhance direct bone contact in rat femoral medullary implants [48-51], and stimulate bone marrow stromal cells and adipose-derived stem cells to regenerate critical size defects [52,53]. To achieve improved bone-related outcomes for bone regeneration *in vivo*, we fabricated a new bone regeneration scaffold, apatite-coated silk-fibroin-based porous biomaterial composite. The composite represents the best of both components, apatite and silk fibroin, in terms of osteoconduction, mechanics, architectural control and slow degradation during new bone formation and remodeling *in vivo*.

A useful scaffold for bone tissue engineering should be biocompatible as well as biodegradable [54,55]. Animal implant surgery is a direct method to assess the bioactivity of tissue engineering materials. The model of bilateral inferior mandibular border defects of canine measuring 2 cm × 1 cm is critical sized, since this defect can not heal spontaneously as we and other researchers have observed [56]. In the present study, no bony-union was observed and the defects were only partly healed with silk scaffolds alone or apatite-coated silk scaffolds alone, and there was no significant difference with new bone volume between the two groups. The newly formed bone both only occurred at the host and bone-material interface and failed to extend toward the center along the scaffold. At the same time, connective tissues grew freely and occupied the intra-scaffold spaces, which impeded host reparative cell ingrowth. Nevertheless, there were no obvious inflammation cells detected. The data clearly demonstrated that both silk scaffolds would not arouse obvious immunoreaction in the animal but by themselves alone failed to repair the critical sized defects whether they were premineralized or not.

Hard tissue engineering may provide a better alternative than currently available bone grafts [57]. To this end, we used the above silk scaffolds to combine with bMSCs for the healing of the mandibular margin defects. The new bone area in two cell-loaded groups increased from the periphery of the parent bone to the inner site of the defects. New bone area and BMD in these tissue engineering groups were significantly enhanced than those in scaffold alone groups. We hypothesis that cells seeded on the scaffolds could filtrate into the pores of the scaffolds and promote new bone formation and mineralization in the inner side without premature fibrillar tissue infiltration, which was demonstrated by histological analysis in cell-loaded groups. These results implies the important role of tissue engineering technique played for bone regeneration in critical sized defects in large animals models.

With regard to the fate and role of the implanted bMSCs, we do not have direct evidence for their *in vivo* fate in this study. However, in a parallel experiment, AdLacZ gene labeled bMSCs combined with apatite-coated silk scaffold were used in a rat mandibular bony defects model, and LacZ expression in the newly formed bone were detected 4 weeks after surgery (data not shown). Long term cell labeling by either retroviral system or lentiviral system are still being explored for further evaluation by the current groups.

As observed, although the seeded cells were distributed throughout the scaffolds, the newly formed bone in the two cell-loaded groups mainly derived from the implant-host tissue interfaces and progressed to the inferior border of the defects. The seeded cells inside the

scaffold may not survive sufficiently to repair such a large critical sized defect. These cells likely recruited host cells to participate in new bone formation and defect repair. One possible mechanism for this recruitment could be explained as follows. First, the seeded cells secreted extracellular matrix, followed by capillary sprouting and vascular invasion into the newly synthesized matrix which brought in additional host cells to promote the healing process [58, 59]. The effect of the apatite coating on the new cells appeared to accelerate the course of osteogenesis. Another likely explanation is that the seeded cells secreted growth factors which could recruit invading reparative cells from the surrounding host tissue engaged in the new bone formation more rapidly and the interaction between cells and the mineral on the scaffold was responsible for this [60,61]. Both mechanisms are likely important during the healing process. Vascularization which is critical for osteogenesis, seeded cells, as well as resident host cells are essential to the repair success of such critical sized defects.

In the current study, once the silk scaffolds were premineralized with apatite and combined with bMSCs in the bMSCs/mSS group, the mandibular border defect was completely repaired and the border of the new bone was close to the normal inferior mandibular border 12 months after transplantation, while the new bone area was less in the bMSCs/SS group. The seeded cells played a critical role in this healing process, however, the apatite coatings were responsible for the improved effects as well. Once the bMSCs were seeded on the scaffold, it would be more favorable for them to differentiate into osteoblasts as well as to secrete extracellular matrix to prevent fibrillar tissue infiltration in the presence of the apatite coatings as demonstrated by SEM [62]. Moreover, the apatite coatings would further affect the resident bMSCs and other host cells to participate in the healing process.

The effect of apatite coatings on osteogenic differentiation of bMSCs has been well documented. Scaffolds impregnated with apatite increased *in vitro* bone nodule formation, as well as *in vivo* bone formation [24], providing an appropriate osteogenic environment for tissue engineering [63]. Chou et al. [47] found apatite coatings promoted osteogenic differentiation through early upregulation of osteopontin (OPN) and later upregulation of osteocalcin (OCN) and bone sialoprotein (BSP) in a 3D model system, relative to noncoated controls. At the same time, the adsorption of growth factors secreted by the seeded bMSCs and other endogenous biologically active molecules to hydroxyapatite is likely different from the plain silk scaffold without the mineral phase [33]. These factors might mediate the cell-scaffold interactions to drive some of the changes in osteoconductivity of the scaffolds. In future studies, the repair mechanism and the effects between the apatite coating and the cells will be further explored to improve control of these interactions to modulate bone tissue regeneration *in vitro* and *in vivo*.

Autogenous bone graft is the gold standard for the repair of bony defects. The autograft repair process is by creeping substitution which involves both resorptive and appositional bone formation [64]. In our study, bony-union was achieved as early as 2 to 3 months after transplantation (data not shown) and better mandibular body shape was observed after sacrifice. We also found the BMD was higher than the normal control mandibles at 12 months post-operation. This indicated the activity of new bone formation and mineralization surpassed the resorption during the repairing process in autogenous bone graft.

The inferior mandibular border defect is a partial defect which do not bear masticatory force directly. So we did not evaluate the biomechanical property of the repaired mandible in this experiment. Further study using apatite-coated silk scaffold for the segmental or load-bearing defects, in which, biomechanical testing should be performed.

Besides the basic requirement for implantable biomaterials, an optimal scaffold for bone engineering should have a suitable degradation rate that can match the rate of new bone

formation and maturation. According to Cancedda's conclusions from large animal studies, optimal resorption time for scaffolds ranged within 12–18 months, a time necessary for the production of a significant amount of new bone [65]. In general, silk fibers lose the majority of their tensile strength within 1 year *in vivo*, and fail to be recognized at the site within 2 years [66]. The absorption of silk *in vivo* could be through proteolytic degradation followed by further metabolism by macrophages and other cells [67-71]. The abundant blood circulation in the oral maxillofacial region could promote the metabolic process. According to Cornell et al. calcium phosphate-rich surface layers can stimulate cell-mediated resorption [72]. We did find that there was more residual silk scaffolds in bMSCs/SS grafts than in the bMSCs/mSS grafts. The apatite coatings may play a special role in silk resorption relevant to macrophages activity, issues that bear further study. Nevertheless, the apatite coated silk scaffold displayed an appropriate degradation rate for sufficient new bone formation when combined with bMSCs during the repairing process. However, comparing with the bMSCs/SS and bMSCs/mSS groups, only little amount of separate pieces of silk scaffolds remained in the defect area in the SS and mSS alone groups. The premature fibrillar tissue infiltration without early new bone deposition may have exposed the scaffold to surrounding body fluid which could accelerate the degradation process [35].

Bone defect studies with both growth factors and cells with scaffolds indicated more effective recovery than cell-loaded scaffolds or scaffold alone repairs. The 1 year residence in this case is comparable with cell seeded repairs in large animal models [73]. The combination of osteoinductive factors, osteogenic cells and apatite coated silk scaffolds for repairing critical sized defects is currently under study to accelerate the healing process and enhance the quality of new bone formation. Meanwhile, a production processes which enables the degradation rates of apatite coated silk biomaterials to match the rate of new bone formation, by adding growth factors and optimizing the materials processing approaches, is also being further explored.

In conclusion, the combination of bMSCs and apatite-coated silk scaffolds can be used as a bone graft to repair canine inferior mandibular border defects when compared to the use of bMSCs/SS and scaffolds alone. The mineralization of silk scaffolds provides increased osteoconductive environment for bMSCs to construct tissue engineered bone to repair mandible defects in large animal.

## Supplementary Material

Refer to Web version on PubMed Central for supplementary material.

## Acknowledgments

The authors appreciate Carmen Preda for fabricating the silk scaffolds, Lunguo Xia, Wenwen Yu, Qing Chang, Dongxia Ye, Duohong Zou, Ling Xu for assistance with animal studies and data collection, as well as Fan Ding for helping statistical analysis. This work was supported by National Natural Science Foundation of China 30400502, 30772431. Program for New Century Excellent Talents in University NCET-08-0353. Science and Technology Commission of Shanghai Municipality 07DZ22007, 08410706400, 08JC1414400, 08DZ2271100, S30206. Shanghai Rising-star Program 05QMX1426, 08QH14017. Shanghai Education Committee Y0203, 07SG19. We also thank NIH DE16710 as well as NIH P41 Tissue Engineering Resource Center and the NIH NIBIB (DK) for support of this study.

## References

1. Taylor GI. The current status of vascularized bone grafts. Clin Plast Surg 1993;10:185. [PubMed: 6340912]
2. Weiland AJ, Phillips TW, Randolph MA. Bone grafts: A radiologic, histologic, and biomechanical model comparing autografts, allografts, and free vascularized bone grafts. Plast Reconstr Surg 1984;74:368. [PubMed: 6382367]

3. Friedlaender GE. Bone allografts: the biological consequences of immunological events. J Bone Joint Surg Am 1991;73:1119–22. [PubMed: 1890114]
4. Nemzek JA, Arnoczky SP, Swenson CL. Retroviral transmission in bone allotransplantation. The effects of tissue processing. Clin Orthop Relat Res 1996;(324):275–82. [PubMed: 8595768]
5. Ma PX, Zhang R, Xiao G, Franceschi R. Engineering new bone tissue *in vitro* on highly porous poly (α-hydroxy acids)/hydroxyapatite composite scaffolds. J Biomed Mater Res 2001;54:284–93. [PubMed: 11093189]
6. Hollinger JO, Leong K. Poly(alpha-hydroxy acids): carriers for bone morphogenetic proteins. Biomaterials 1996;17:187–94. [PubMed: 8624395]
7. Albrektsson T, Johansson C. Osteoinduction, osteoconduction and osseointegration. Eur Spine J 2001;10(Suppl 2):S96–S101. [PubMed: 11716023]
8. DeLustro F, Dasch J, Keefe J, Ellingsworth L. Immune responses to allogeneic and xenogeneic implants of collagen and collagen derivatives. Clin Orthop 1990;(260):263–79. [PubMed: 2225633]
9. Luginbuehl V, Meinel L, Merkle HP, Gander B. Localized delivery of growth factors for bone repair. Eur J Pharm Biopharm 2004;58:197–208. [PubMed: 15296949]
10. Hollinger JO, Brekke J, Gruskin E, Lee D. Role of bone substitutes. Clin Orthop 1996;(324):55–65. [PubMed: 8595778]
11. Athanasiou KA, Niederauer GG, Agrawal CM. Sterilization, toxicity, biocompatibility and clinical applications of polylactic acid/polyglycolic acid copolymers. Biomaterials 1996;17:93–102. [PubMed: 8624401]
12. Suh H. Recent advances in biomaterials. Yonsei Med J 1998;39:87–96. [PubMed: 9587247]
13. Harris LD, Kim BS, Mooney DJ. Open pore biodegradable matrices formed with gas foaming. J Biomed Mater Res 1998;42:396–402. [PubMed: 9788501]
14. Wang M. Developing bioactive composite materials for tissue replacement. Biomaterials 2003;24:2133–51. [PubMed: 12699650]
15. Sarkar BK. Fatigue of brittle materials — a critical appraisal. Bull Mater Sci 1995;18:755–72.
16. Higashi S, Yamamuro T, Nakamura T, Ikada Y, Hyon SH, Jamshidi K. Polymer-hydroxyapatite composites for biodegradable bone fillers. Biomaterials 1986;7:183–87. [PubMed: 3013326]
17. Verheyen CC, de Wijn JR, van Blitterswijk CA, de Groot K. Evaluation of hydroxylapatite/poly(L-lactide) composites: Mechanical behavior. J Biomed Mater Res 1992;26:1277–96. [PubMed: 1331112]
18. Kikuchi M, Suetsugu Y, Tanaka J, Akao M. Preparation and mechanical properties of calcium phosphate/copoly-L-lactide composites. J Mater Sci Mater Med 1997;8:361–64. [PubMed: 15348736]
19. Devin JE, Attawia MA, Laurencin CT. Three-dimensional degradable porous polymer-ceramic matrices for use in bone repair. J Biomater Sci Polym Ed 1996;7:661–99. [PubMed: 8639475]
20. Thomson RC, Yaszemski MJ, Powers JM, Mikos AG. Hydroxyapatite fiber reinforced poly a-hydroxy ester foams for bone regeneration. Biomaterials 1998;19:1935–43. [PubMed: 9863527]
21. Ambrosio AM, Sahota JS, Khan Y, Laurencin CT. A novel amorphous calcium phosphate polymer ceramic for bone repair: I. Synthesis and characterization. J Biomed Mater Res 2001;58:295–301. [PubMed: 11319744]
22. Marra KG, Szem JW, Kumta PN, DiMilla PA, Weiss LE. *In vitro* analysis of biodegradable polymer blend/hydroxyapatite composites for bone tissue engineering. J Biomed Mater Res 1999;47:324–35. [PubMed: 10487883]
23. Durham SR, McComb JG, Levy ML. Correction of large (>25 cm(2)) cranial defects with “reinforced” hydroxyapatite cement: technique and complications. Neurosurgery 2003;52:842–45. 845. discussion. [PubMed: 12657179]
24. Bourgeois B, Laboux O, Obadia L, Gauthier O, Betti E, Aguado E, et al. Calcium-deficient apatite: a first *in vivo* study concerning bone ingrowth. J Biomed Mater Res 2003;65A:402–08.
25. Neo M, Kotani S, Nakamura T, Yamamuro T, Ohtsuki C, Kokubo T, et al. A comparative study of ultrastructures of the interfaces between four kinds of surface-active ceramic and bone. J Biomed Mater Res 1992;26:1419–32. [PubMed: 1447227]

26. van Blitterswijk CA, Hesseling SC, Grote JJ, Koerten HK, de Groot K. The biocompatibility of hydroxyapatite ceramic: a study of retrieved human middle ear implants. J Biomed Mater Res 1990;24:433–53. [PubMed: 2161412]
27. Le Huec JC, Schaeverbeke T, Clement D, Faber J, Le Rebeller A. Influence of porosity on the mechanical resistance of hydroxyapatite ceramics under compressive stress. Biomaterials 1995;16:113–18. [PubMed: 7734643]
28. Meinel L, Hofmann S, Karageorgiou V, Zichner L, Langer R, Kaplan D, et al. Engineering cartilage-like tissue using human mesenchymal stem cells and silk protein scaffolds. Biotechnol Bioeng 2004;88:379–91. [PubMed: 15486944]
29. Jin HJ, Chen J, Karageorgiou V, Altman GH, Kaplan DL. Human bone marrow stromal cell responses on electrospun silk fibroin mats. Biomaterials 2004;25:1039–47. [PubMed: 14615169]
30. Meinel L, Karageorgiou V, Fajardo R, Snyder B, Shinde-Patil V, Zichner L, et al. Bone tissue engineering using human mesenchymal stem cells: effects of scaffold material and medium flow. Ann Biomed Eng 2004;32:112–22. [PubMed: 14964727]
31. Meinel L, Karageorgiou V, Hofmann S, Fajardo R, Snyder B, Li C, et al. Engineering bone-like tissue *in vitro* using human bone marrow stem cells and silk scaffolds. J Biomed Mater Res 2004;25:71A.
32. Meinel L, Hofmann S, Karageorgiou V, Kirker-Head C, McCool J, Gronowicz G, et al. The inflammatory responses to silk films *in vitro* and *in vivo*. Biomaterials 2005;26:147–55. [PubMed: 15207461]
33. Kim HJ, Kim UJ, Kim HS, Li C, Wada M, Leisk GG, Kaplan DL. Bone tissue engineering with premineralized silk scaffolds. Bone 2008;42:1226–34. [PubMed: 18387349]
34. Sun XJ, Zhang ZY, Wang SY, Gittens SA, Jiang XQ, Chou LL. Maxillary sinus floor elevation using a tissue-engineered bone complex with osteobone and bMSCs in rabbits. Clin Oral Implants Res 2008;19(8):804–13. [PubMed: 18705812]
35. Wang S, Zhang Z, Zhao J, Zhang X, Sun X, Xia L, et al. Vertical alveolar ridge augmentation with beta-tricalcium phosphate and autologous osteoblasts in canine mandible. Biomaterials 2009;30(13): 2489–98. [PubMed: 19147220]
36. Sofia S, McCarthy MB, Gronowicz G, Kaplan DL. Functionalized silk-based biomaterials for bone formation. J Biomed Mater Res 2001;54:139–48. [PubMed: 11077413]
37. Li C, Vepari C, Jin HJ, Kim HJ, Kaplan DL. Electrospun silk-BMP-2 scaffolds for bone tissue engineering. Biomaterials 2006;27:3115–24. [PubMed: 16458961]
38. Kim HJ, Kim UJ, Vunjak-Novakovic G, Min BH, Kaplan DL. Influence of macroporous protein scaffolds on bone tissue engineering from bone marrow stem cells. Biomaterials 2005;26:4442–52. [PubMed: 15701373]
39. Li C, Jin H, Botsaris GD, Kaplan DL. Silk apatite composites from electrospun fibers. J Mater Res 2005;20:3374–84.
40. Inoue S, Tanaka K, Arisaka F, Kimura S, Ohtomo K, Mizuno S. Silk fibroin of Bombyx mori is secreted, assembling a high molecular mass elementary unit consisting of H-chain, L-chain, and P25, with a 6:6:1 molar ratio. J Biol Chem 2000;275:40517–28. [PubMed: 10986287]
41. Tanaka K, Inoue S, Mizuno S. Hydrophobic interaction of P25, containing Asn-linked oligosaccharide chains, with the H-L complex of silk fibroin produced by Bombyx mori. Insect Biochem Mol Biol 1999;29:269–76. [PubMed: 10319440]
42. Wang Y, Kim HJ, Vunjak-Novakovic G, Kaplan DL. Stem cell-based tissue engineering with silk biomaterials. Biomaterials 2006;27:6064–82. [PubMed: 16890988]
43. Altman GH, Diaz F, Jakuba C, Calabro T, Horan RL, Chen J, et al. Silk-based biomaterials. Biomaterials 2003;24:401–16. [PubMed: 12423595]
44. Cunniff PM, Fossey SA, Auerbach MA, Song JW, Kaplan DJ, Adams WW, et al. Mechanical and thermal properties of the dragline silk from the spider Nephila claviceps. Polym Adv Technol 1994;5:401–10.
45. Meinel L, Fajardo R, Hofmann S, Langer R, Chen J, Snyder B, et al. Silk implants for the healing of critical size bone defects. Bone 2005;37:688–98. [PubMed: 16140599]
46. Meinel L, Betz O, Fajardo R, Hofmann S, Nazarian A, Cory E, et al. Silk based biomaterials to heal critical sized femur defects. Bone 2006;39:922–31. [PubMed: 16757219]

47. Chou YF, Dunn JC, Wu BM. *In vitro* response of MC3T3-E1 pre-osteoblasts within three-dimensional apatite-coated PLGA scaffolds. J Biomed Mater Res B Appl Biomater 2005;75:81–90. [PubMed: 16001421]
48. Yan WQ, Nakamura T, Kawanabe K, Nishigochi S, Oka M, Kokubo T. Apatite layer-coated titanium for use as bone bonding implants. Biomaterials 1997;18:1185–90. [PubMed: 9259516]
49. Li P. Biomimetic nano-apatite coating capable of promoting bone ingrowth. J Biomed Mater Res 2003;66A:79–85.
50. Barrère F, van der Valk CM, Meijer G, Dalmeijer RA, de Groot K, Layrolle P. Osteointegration of biomimetic apatite coating applied onto dense and porous metal implants in femurs of goats. J Biomed Mater Res 2003;67B:655–65.
51. Kuroda S, Virdi AS, Li P, Healy KE, Sumner DR. A lowtemperature biomimetic calcium phosphate surface enhances early implant fixation in a rat model. J Biomed Mater Res 2004;70A:66–73.
52. Ohgushi H, Caplan AI. Stem cell technology and bioceramics: from cell to gene engineering. J Biomed Mater Res 1999;48:913–27. [PubMed: 10556859]
53. Cowan CM, Shi YY, Aalami OO, Chou YF, Mari C, Thomas R, et al. Adipose-derived adult stromal cells heal critical-size mouse calvarial defects. Nature Biotech 2004;22:560–67.
54. Vacanti CA. The impact of biomaterials research on tissue engineering. MRS Bull 2001;26:798–99.
55. Ripamonti U, Duneas N. Tissue engineering of bone by osteoinductive biomaterials. MRS Bull 1996;21:36–39.
56. Gerard D, Carlson ER, Gotcher JE, Jacobs M. Effects of platelet-rich plasma on the healing of autologous bone grafted mandibular defects in dogs. J Oral Maxillofac Surg 2006;64:443–51. [PubMed: 16487807]
57. Petrovic L, Schlegel AK, Schultze-Mosgau S, Wiltfang J. Different substitute biomaterials as potential scaffolds in tissue engineering. Int J Oral Maxillofac Implants 2006;21:225–31. [PubMed: 16634492]
58. Ripamonti U. Soluble osteogenic molecular signals and the induction of bone formation. Biomaterials 2006;27:807–22. [PubMed: 16213014]
59. Lee SY, Miwa M, Sakai Y, Kuroda R, Matsumoto T, Iwakura T, et al. In vitro multipotentiality and characterization of human unfractured traumatic hemarthrosis derived progenitor cells: a potential cell source for tissue repair. J Cell Physiol 2007;3:561–66. [PubMed: 17171634]
60. Urist MR. Bone: formation by autoinduction. Science 1965;150:893–99. [PubMed: 5319761]
61. Rickard DJ, Sullivan TA, Shencker BJ, Leboy PS, Kazhdan I. Induction of rapid osteoblast differentiation in rat bone marrow stromal cell cultures by dexamethasone and BMP-2. Dev Biol 1994;161:218–28. [PubMed: 8293874]
62. Li P. Biomimetic nano-apatite coating capable of promoting bone ingrowth. J Biomed Mater Res 2003;66A:79–85.
63. Rosa AL, Beloti MM, Van Noort R, Hatton PV, Devlin AJ. Surface topography of hydroxyapatite affects ROS17/2.8 cells response. Pesqui Odontol Bras 2002;16:209–15. [PubMed: 12386681]
64. Burchardt H. The biology of bone graft repair. Clin Orthop Relat Res 1983;174:28–42. [PubMed: 6339139]
65. Cancedda R, Giannoni P, Mastrogiacomo M. A tissue engineering approach to bone repair in large animal models and in clinical practice. Biomaterials 2007;28:4240–50. [PubMed: 17644173]
66. Ethicon, Inc.. Wound closure manual. Somerville,NJ: Ethicon, Inc.; The suture: specific suturing materials. Non-absorbable sutures. copyright 2000,Chapter 2
67. Rossitch E Jr, Bullard DE, Oakes WJ. Delayed foreign-body reaction to silk sutures in pediatric neurosurgical patients. Childs Nerv Syst 1987;3:375–78. [PubMed: 3329961]
68. Soong HK, Kenyon KR. Adverse reactions to virgin silk sutures in cataract surgery. Ophthalmology 1984;91:479–83. [PubMed: 6377167]
69. Lam KH, Nijenhuis AJ, Bartels H, Postema AR, Jonkman MF, Pennings AJ, et al. Reinforced poly (l-Lactic Acid) fibers as suture material. J Appl Biomater 1995;6:191–97. [PubMed: 7492810]
70. Salthouse TN, Matlaga BF, Wykoff MH. Comparative tissue response to six suture materials in rabbit cornea,sclera,and ocular muscle. Am J Ophthalmol 1977;84:224–33. [PubMed: 888893]
71. Wang Y, Rudym DD, Walsh A, Abrahamsen L, Kim HJ, Kim HS, et al. *In vivo* degradation of three-dimensional silk fibroin scaffolds. Biomaterials 2008;29:3415–28. [PubMed: 18502501]

72. Cornell CN. Osteoconductive materials and their role as substitutes for autogenous bone grafts. Orthop Clin North Am 1999;30:591–98. [PubMed: 10471764]

73. Mastrogiacomo M, Corsi A, Francioso E, Di Comite M, Monetti F, Scaglione S, et al. Reconstruction of extensive long bone defects in sheep using resorbable bioceramics based on silicon stabilized tricalcium phosphate. Tissue Eng 2006;5:1261–73. [PubMed: 16771639]

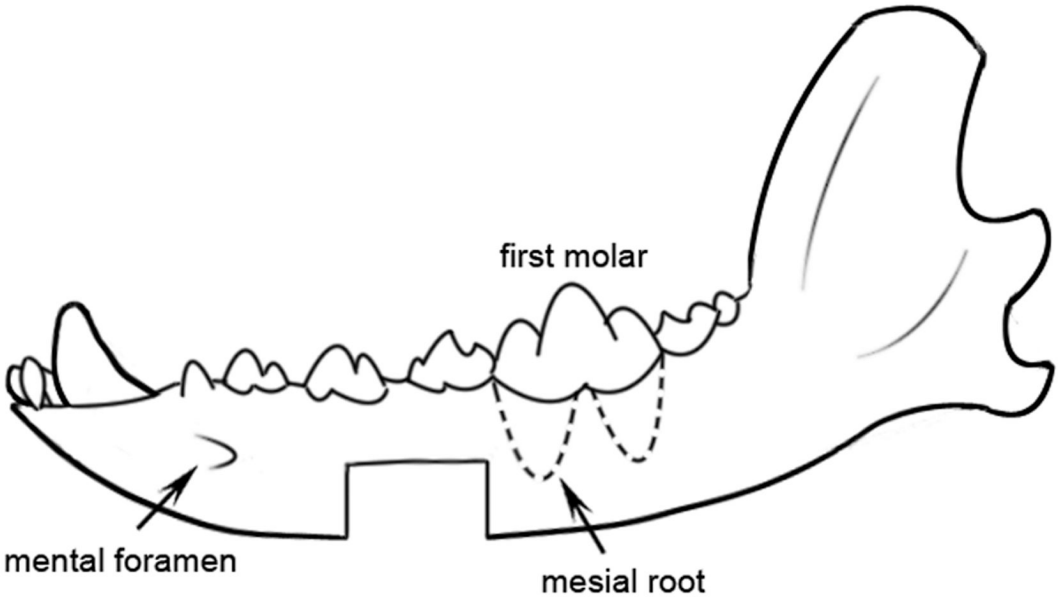


**Fig. 1.**
Schematic illustration of region of interest (ROI) position. The position of the defect located was under the premolar and between the mental foramen and the mesial root of the first molar.

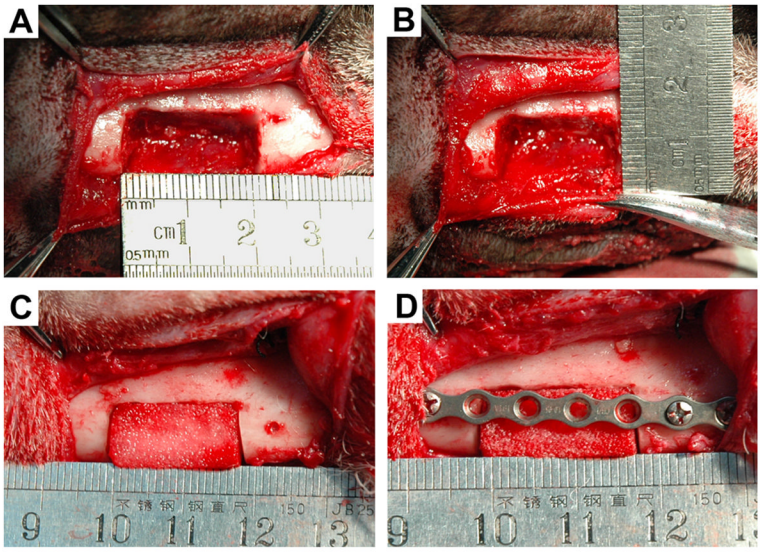


**Fig. 2.**

Surgical procedure. Bilateral inferior mandibular border full-thickness defects were made measuring 2cm × 1cm (A,B). The defect was filled with bMSCs/mSS construct (C). The titanium plate was secured in place with screws (D).

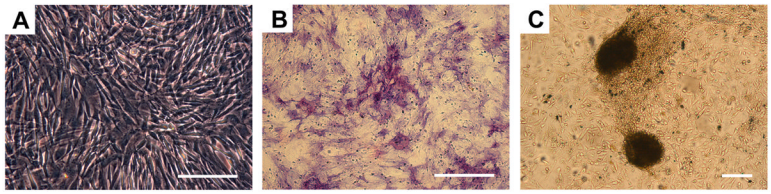


**Fig. 3.**
The expanded bMSCs displayed the typical spindle-shaped fibroblastic phenotype (A). Alkaline phosphatase-positive staining area (B) and von Kossa-positive staining (C) 14 days after induction with dexamethasone. Scale bar = 100 μm.

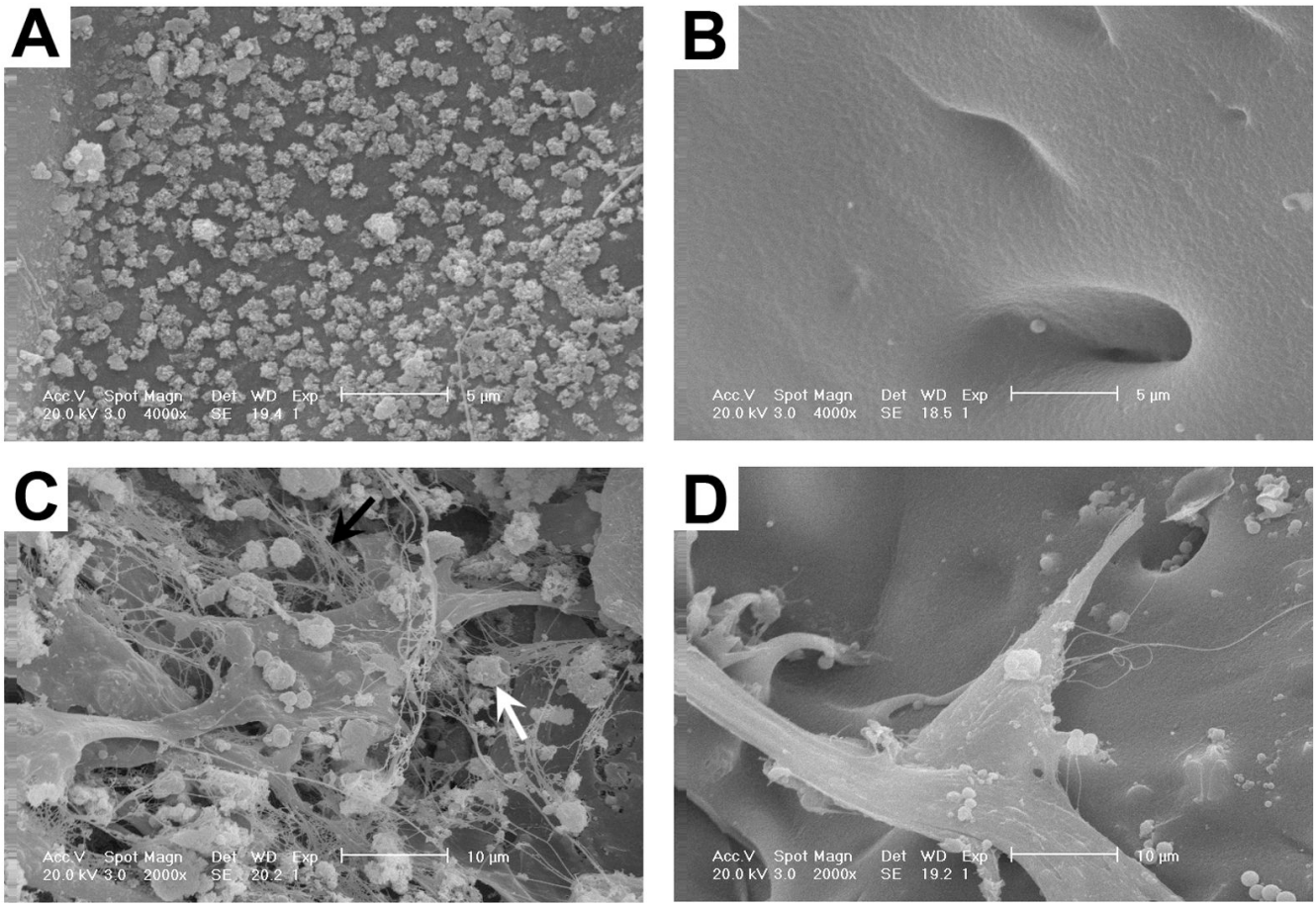


**Fig. 4.**

SEM evaluation of scaffold microstructure and cell interactions. Apatite coating was visible on the surface of mineralized silk scaffold **(A)** compared with the plain silk scaffold **(B)**. Scale bar = 5 μm. BMSCs reached confluence with abundant fibril networks of extracellular matrix and mineralized nodules deposited on apatite-coated scaffolds **(C)**. Less extracellular matrix and no obvious mineralized nodules formed on the non-coated scaffolds **(D)**. Black arrow shows extracellular matrix; white arrow shows mineralized nodules. Scale bar = 10 μm.

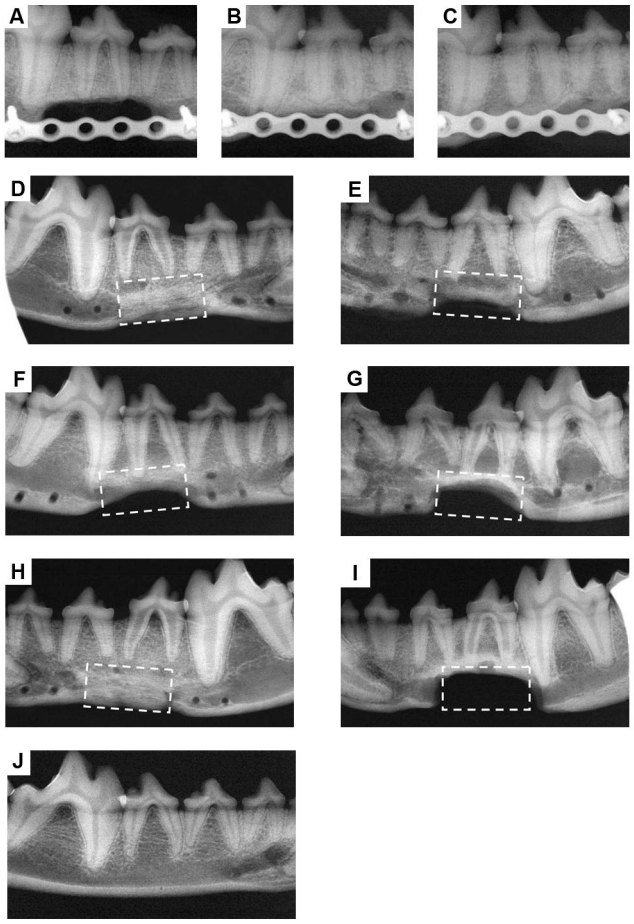


**Fig. 5.**

Radiographs of treated defects taken at different time points post-operation. In the bMSCs/mSS group, little calluses formed at 1 month post-operation (A), and more calluses were observed at 3 months post-operation (B). The volume and radiopacity of newly formed bone were highly increased at 6 months post-operation (C). At 12 months post-operation, the radiopaque shadow had completely filled the defect site (D). In the bMSCs/SS group, the newly formed bone failed to fill the defects completely even at 12 months post-operation (E). At 12 months, only little calluses could be observed near the defect margin in the mSS alone group (F) and SS alone group (G). In the autograft group, high radiopacity of autogenous bone with newly formed bone was achieved at 12 months post-operation (H). Untreated defects did not repair at 12 months in the blank control group (I). Radiograph of normal mandible (J).

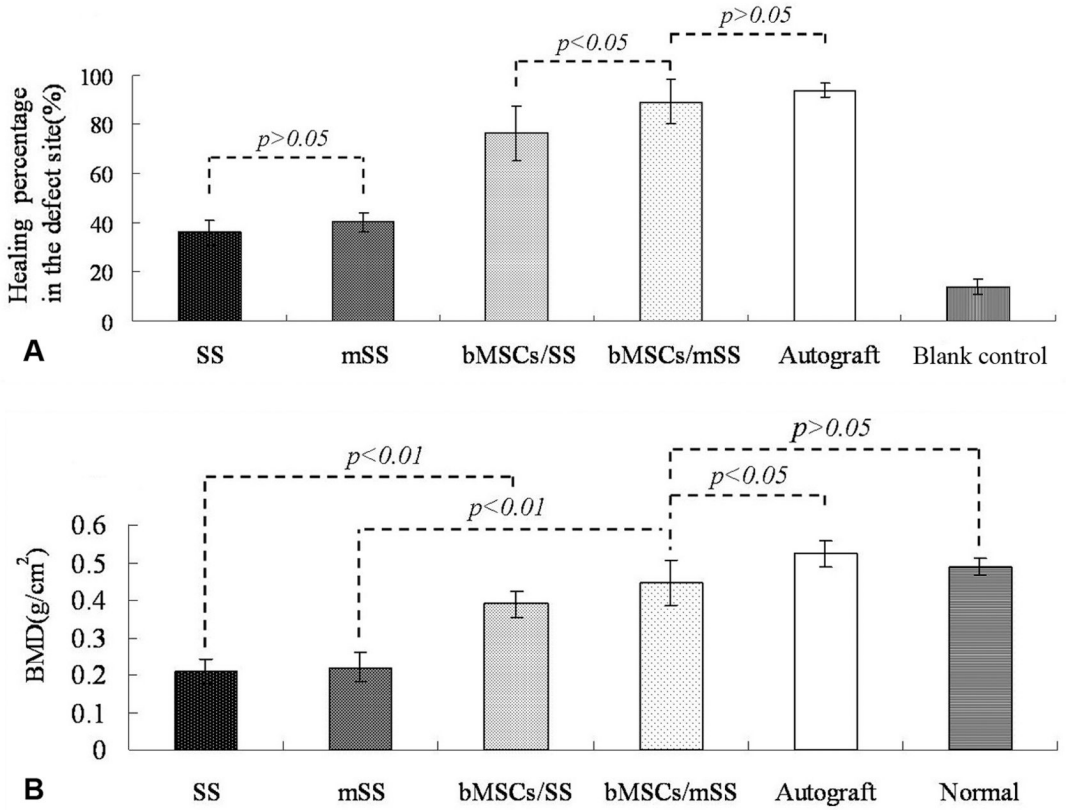


**Fig. 6.**

Statistical analysis of the healed areas (A) and local bone mineral densities (B) analysis by dual energy X-ray absorptiometry of each group at 12 months post-operation.

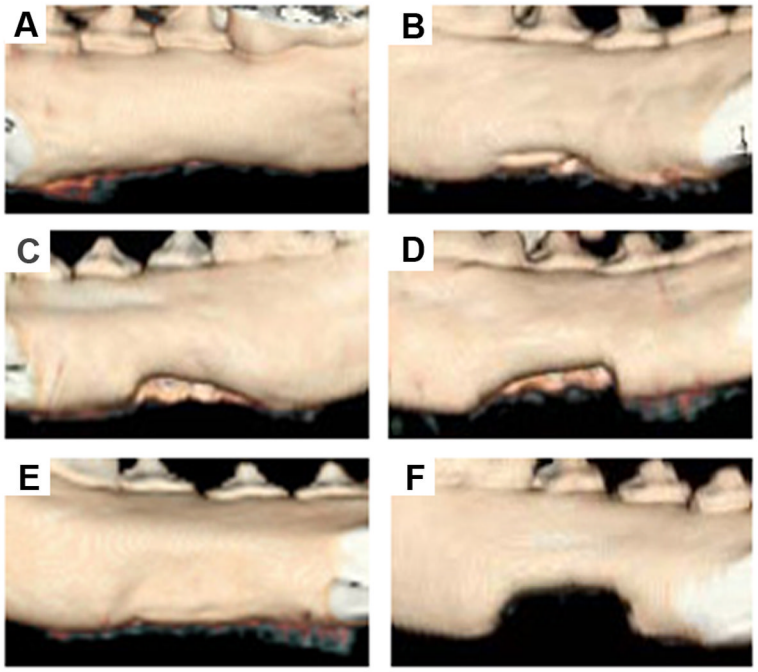


**Fig. 7.**

3D-CT images of treated mandibles at lingual side 12 months post-operation. In the bMSCs/mSS group, the mandible defects were completely repaired (A), while the inferior of the defects in the bMSCs/SS group failed to repair completely (B). In the mSS (C) and SS (D) alone groups, the mandible defects were partially repaired at the margin side. As a positive control, in the autograft group integrity of the mandibular borders shape were observed (E). In the blank control, untreated defects did not repair (F).

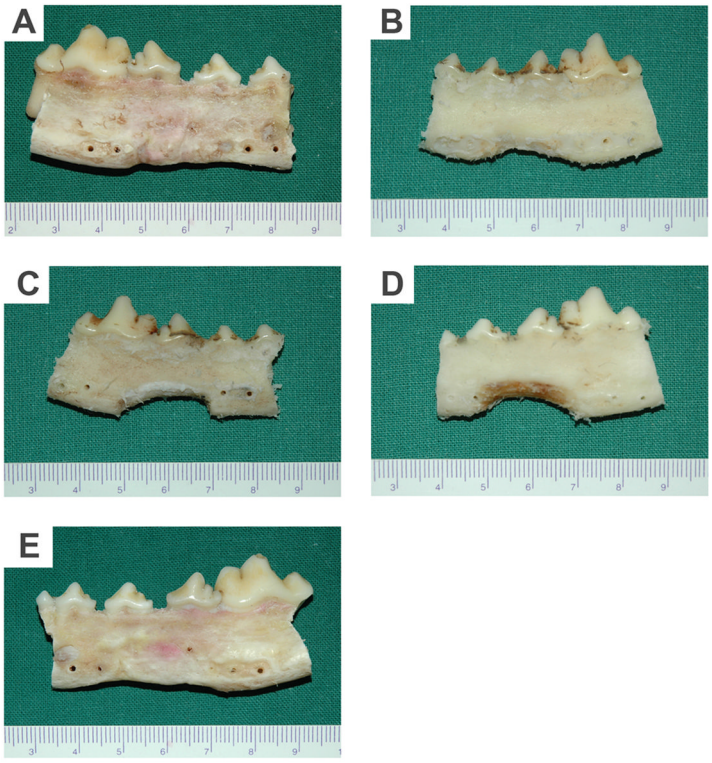


**Fig. 8.**
Gross view of repaired mandibles at buccal side 12 months post-operation. In the bMSCs/mSS (A) or autograft group (E), the mandible contours were reconstructed. In the bMSCs/SS group (B), the inferior of the defects remained unfilled completely. In the mSS (C) or SS (D) groups, respectively, bony callus were poorly formed at the defect margins.

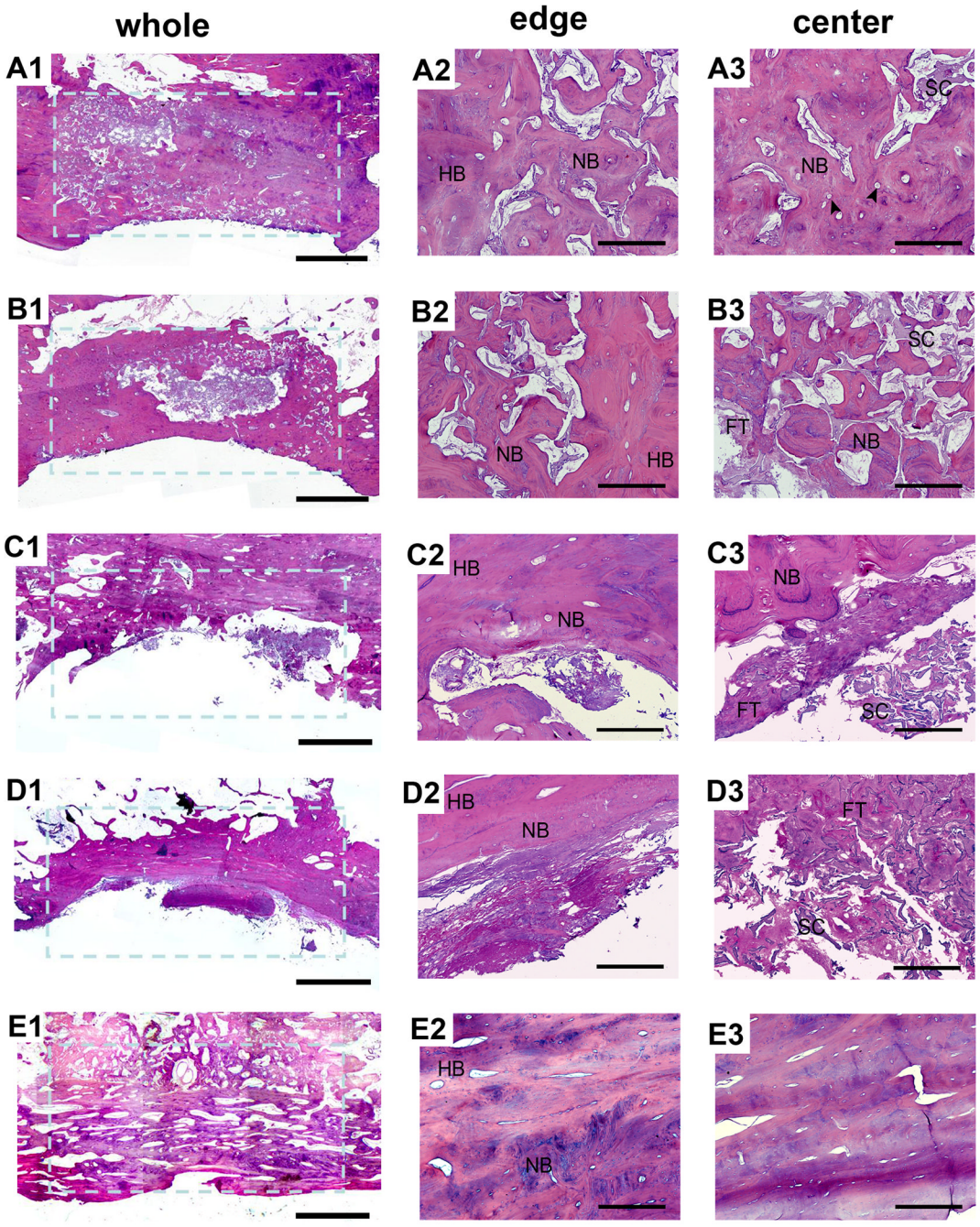


**Fig. 9.**

The whole and local photomicrograph of histologic images of repaired mandibles at 12 months post-operation. In the bMSCs/mSS group, substantial new bone formation was observed within the defect site and most scaffolds had degraded into small pieces (A1). New bone formation was observed without a clear boundary between newly formed tissue engineered bone and native bone (A2). Silk scaffolds lost their structural integrity with separate small pieces left and were almost filled by irregular osteon formation in the repaired area. Blood vessels were formed accompanying with the bone ingrowth (A3). In the bMSCs/SS group, new bone formation was observed with a mass of residual silk scaffold at the center of the defect site (B1). Silk scaffolds held their pore structure and failed to be filled with enough newly formed

bone (B2, B3). In the mSS (C1-C3) and SS (D1-D3) groups, new bone only formed at the periphery and the scaffolds of these two groups failed to completely degraded. In the autograft group, a bony-union was observed (E1) without clear boundary and mature lamellar bone were observed (E2, E3). FT: fibrous tissue; HB: host bone; NB: new bone; SC: scaffold. Arrow head shows blood vessels. Scale bar = 0.5 cm in A1-E1. Scale bar = 500 μm in A2-E2 and A3-E3.

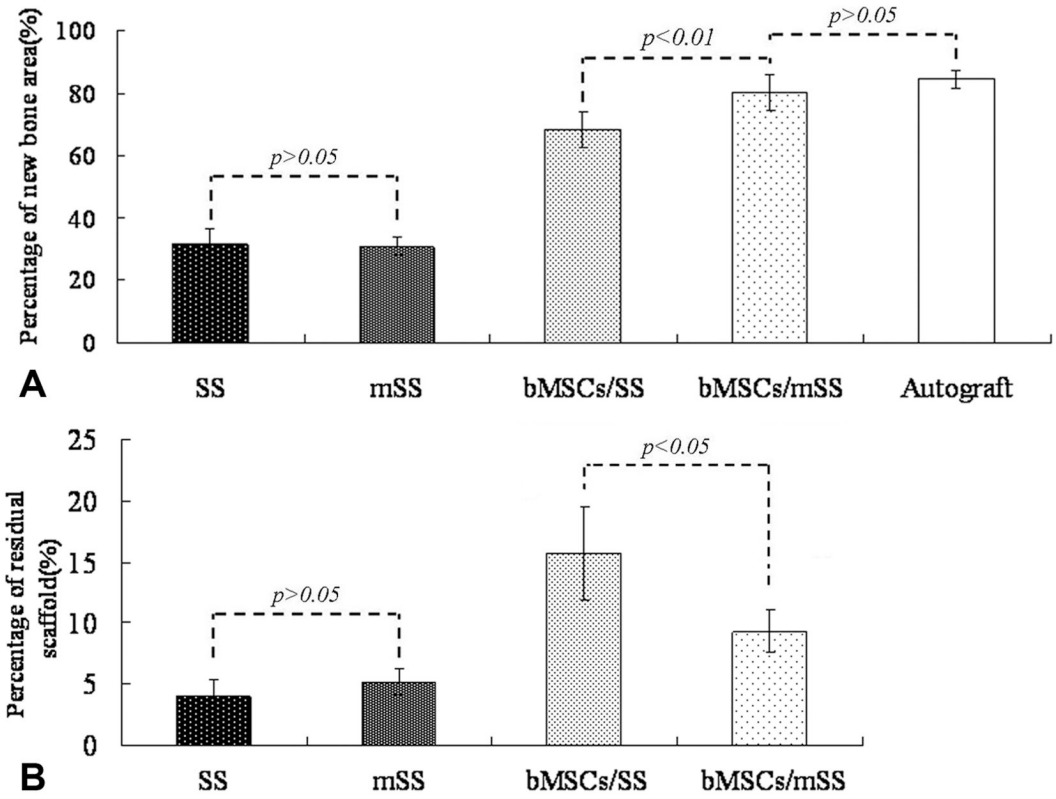


**Fig. 10.**

Percentage of new bone area (A) and residual scaffold (B) assessed in each group using histomorphometry. The quantity of newly formed bone for bMSCs/mSS group was much higher than that in the bMSCs/SS group ($p<0.01$) and no significant difference was found as compared with the autograft group ($p>0.05$). The percentage of residual scaffold was less in the bMSCs/mSS group than that in the bMSCs/SS group ($p<0.05$), and less in scaffold alone groups than that in cell-loaded groups ($p<0.05$).